EUROPEAN ORGANIZATION FOR NUCLEAR RESEARCH

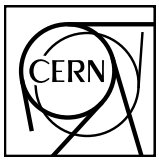

ALICE-PUBLIC-2016-002

ALICE luminosity determination for pp collisions at $\sqrt{s}$ = 13 TeV

ALICE Collaboration*

Abstract

Luminosity determination in ALICE is based on visible cross sections measured in van der Meer scans. In 2015, the Large Hadron Collider provided proton-proton collisions at a centre-of-mass energy of $\sqrt{s}$ = 13 TeV. A van der Meer scan was performed in August 2015, where the cross section was measured for two classes of visible interactions, based on particle detection in the ALICE luminometers: the T0 detector with pseudorapidity coverage $4.6 < \eta < 4.9$, $-3.3 < \eta < -3.0$ and the V0 detector with pseudorapidity coverage $2.8 < \eta < 5.1$, $-3.7 < \eta < -1.7$. This document describes the experimental set-up and the analysis procedure used for such a measurement. In addition, the long-term stability and consistency of the vdM-based calibration of the luminometers is discussed.

*See Appendix A for the list of collaboration members

1 Introduction

Luminosity determination in ALICE (A Large Ion Collider Experiment) [1] at the Large Hadron Collider (LHC) is based on visible cross sections measured in van der Meer (vdM) scans [2, 3]. The visible cross section $\sigma_{\rm vis}$ seen by a given detector (or set of detectors) with a given trigger condition is a fraction of the total inelastic interaction cross section $\sigma_{\rm inel}$: $\sigma_{\rm vis} = \varepsilon\sigma_{\rm inel}$, where ε is the fraction of inelastic events that satisfy the trigger condition. In the following, a class of inelastic events satisfying a given trigger condition will be referred to as a reference process, and the detector providing the trigger signal will be referred to as a luminometer. Once the reference-process cross section ($\sigma_{\rm vis}$) is measured, the luminosity at the ALICE interaction point (IP2) is determined as the reference-process rate divided by $\sigma_{\rm vis}$. This procedure does not require a knowledge of ε.

In standard vdM scans the two beams are moved across each other in the transverse directions x (horizontal) and y (vertical). The x and y scans are performed separately, the beams being head-on in the non-scanned direction. Measurement of the rate R of the reference process as a function of the beam separation Δx, Δy allows one to determine the luminosity L for head-on collisions of a pair of bunches with particle intensities N_1 and N_2 as

$$L = N_1 N_2 f_{\rm rev}/(h_x h_y), \tag{1}$$

where $f_{\rm rev}$ is the accelerator revolution frequency and h_x and h_y are the effective convolved beam widths in the two transverse directions. h_x and h_y are measured as the area below the $R(\Delta x, 0)$ and $R(0, \Delta y)$ curve (scan area), respectively, each divided by the head-on rate $R(0,0)$. The cross section $\sigma_{\rm vis}$ for the chosen reference process is then

$$\sigma_{\rm vis} = R(0,0)/L. \tag{2}$$

The formalism of equation 1 assumes complete factorisation of the beam profiles in the two transverse directions, such that the beam overlap region is fully described by the product $h_x h_y$. Previous studies performed at the LHC [4–6] have shown that factorisation can be broken to a non-negligible level. Such non-factorisation effects can be studied and quantified by measuring the luminous region parameters via the distribution of interaction vertices, as a function of the beam separation.

In 2015, the LHC provided proton-proton (pp) collisions at a centre-of-mass energy of $\sqrt{s}$ = 13 TeV. A van der Meer scan was performed August 25^{th}-26^{th} (LHC fill 4269), and the cross section was measured for two reference processes. In Sec. 2 the detectors used for the measurement are briefly described, along with the relevant machine parameters and the adopted scan procedure. In Sec. 3 the vdM scan analysis procedure is described. In Sec. 4 the results and uncertainties for the visible cross-section measurement are presented and discussed. In Sec. 5 the application of the vdM scan results to the measurement of the integrated luminosity is discussed, with particular emphasis to the stability in time and consistency of the luminosity signals.

2 Experimental setup

In the August vdM scan, the cross section was measured for two reference processes: one is based on the V0 detector, the other on the T0 detector. A detailed description of these detectors is given in [1], and their performance is discussed in [7], [8] and [9]. The V0 detector consists of two hodoscopes, with 32 scintillator tiles each, located on opposite sides of the IP2, at distances of 340 cm (V0A) and 90 cm (V0C) along the beam axis, covering the pseudorapidity (η) ranges $2.8 < \eta < 5.1$ (V0A) and $-3.7 < \eta < -1.7$ (V0C). The T0 detector consists of two arrays of 12 Cherenkov counters each, located on opposite sides of IP2, at distances of 370 cm (T0A) and 70 cm (T0C) along the beam axis, covering the pseudorapidity ranges $4.6 < \eta < 4.9$ (T0A) and $-3.3 < \eta < -3.0$ (T0C). Note that the clockwise-travelling LHC beam moves from side A to side C. The C side is the one hosting the ALICE muon arm [1].

The V0-based trigger condition, chosen as the reference process, requires at least one hit in each detector hodoscope, i.e. on both sides of IP2. A similar trigger condition defines the T0-based reference process, with the additional condition that the longitudinal coordinate of the interaction vertex, evaluated by the trigger electronics via the difference of arrival times in the two arrays (measured with a resolution of 20 ps), lies in the range $|z| < 30$ cm (where $z = 0$ is the nominal IP2 position). This online cut aims to reject the background from beam-gas and beam-satellite interactions. The cut value of 30 cm is much larger than the RMS longitudinal size of the interaction region ($\simeq$ 4-5 cm), making signal loss induced by the cut negligible ($<10^{-5}$).

During the vdM scan session, each proton beam consisted of 51 bunches and 27 bunch pairs were colliding at IP2. The minimum spacing between two consecutive bunches in each beam was 1 μs. The β^* value[1] at IP2 was 19 m. The nominal (half) vertical crossing angle of the two beams at IP2 was -195 μrad, the minus sign indicating that the two beams exit the crossing region with negative y coordinate with respect to the beam axis. The current in the ALICE solenoid (dipole) was 30 kA (6 kA), corresponding to a field strength of 0.5 T (0.7 T). The maximum beam separation during the scan was about 0.6 mm, corresponding to about six times the RMS of the transverse beam profile ($\sigma_{\rm beam}$). The reference-process rates were recorded (and the cross section measured) separately for each colliding bunch pair. Two independent measurements per bunch pair were performed by repeating the (horizontal and vertical) scan pair twice. In addition, a length-scale calibration scan was performed, whose purpose will be discussed in Sec. 3. Finally, a vdM scan with non-zero separation (offset) in the non-scanned direction was performed, to provide additional input for non-factorisation studies. The offset amounts to about 2 $\sigma_{\rm beam}$. The scan sequence is illustrated in Fig. 1, which shows the total rate of the T0- and V0-based trigger signals as a function of time during the scan session.

The proton bunch intensities were on the order of 8-10$\times 10^{10}$ p/bunch. The bunch-intensity measurement is provided by the LHC instrumentation [10]: a DC current transformer (DCCT), measuring the total beam intensity, and a fast beam current transformer (fBCT), measuring the relative bunch populations. The measured beam intensity is corrected for the fraction of ghost and satellite charges[2]. A measurement of ghost charge is provided independently by the LHCb collaboration, via the rate of beam-gas collisions occurring in nominally empty bunch slots, as described in [12], and by the LHC Longitudinal Density Monitor (LDM), which measures synchrotron radiation photons emitted by the beams [13]. The resulting ghost-charge correction factor to the bunch-intensity product N_1N_2 is 0.9985$\pm$0.0004, where the uncertainty includes the difference between the two measurements. The LDM provides in addition a measurement of the satellite-charge fraction, which was found to be negligible ($< 0.05\%$).

3 Data analysis

Three steps are needed to convert the raw T0 and V0 trigger rates of Fig. 1 into the actual reference process rates. First, the contamination by beam–satellite and beam–gas interactions in the V0 rate is removed using the detector timing measurements. The background is identified via the sum and difference of arrival times in the two V0 arrays from offline analysis of the data collected during the scan [7, 14]. The arrival times are obtained by averaging over the signal times of all hits of each array. The background contamination is measured as the fraction of events in which the sum and difference of times lie outside of a window of $\pm$3 ns around the values expected for beam-beam collisions. The measurement is performed for each separation value and the corresponding raw rate is corrected by the obtained fraction.

[1] The $\beta(z)$ function describes the single-particle motion and determines the variation of the beam envelope as a function of the coordinate along the beam orbit (z). The notation β^* denotes the value of the β function at the interaction point.

[2] The radio-frequency (RF) configuration of the LHC is such that the accelerator orbit is divided in 3564 slots of 25 ns each. Each slot is further divided in ten buckets of 2.5 ns each. In nominally filled slots, the particle bunch is captured in the central bucket of the slot. Following the convention established in [11], the charge circulating outside of the nominally filled slots is referred to as ghost charge; the charge circulating within a nominally filled slot but not captured in the central bucket is referred to as satellite charge.

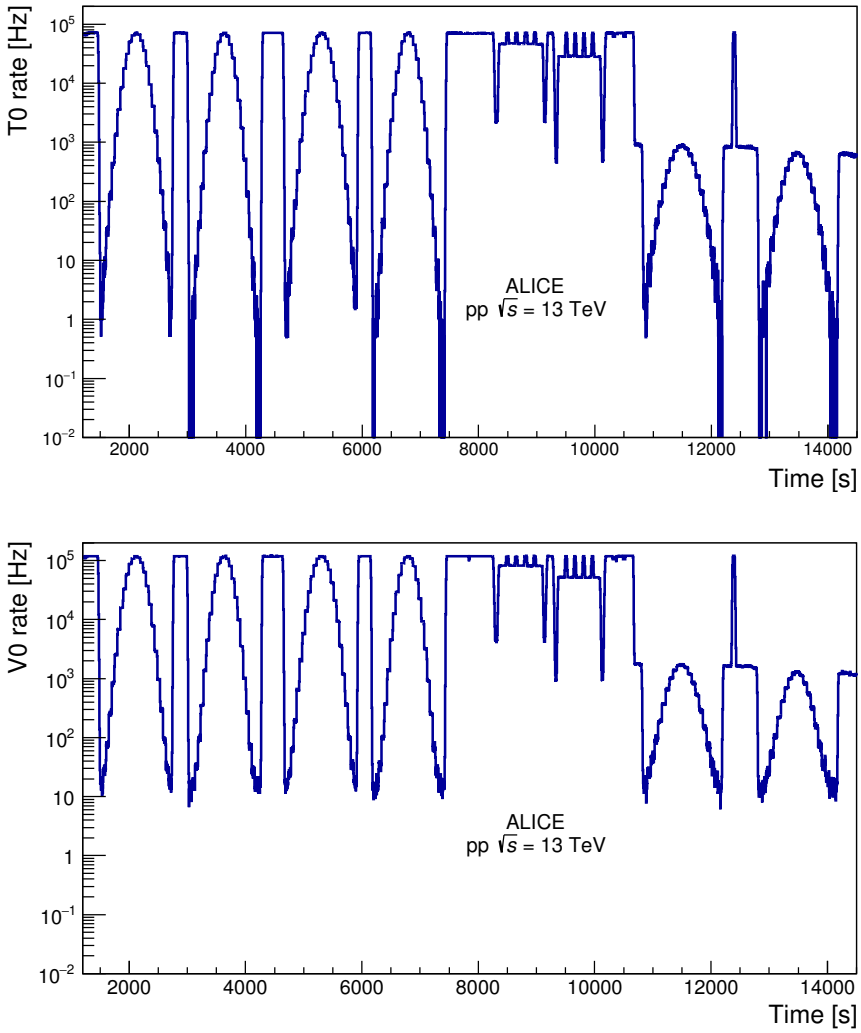

Fig. 1: Raw, bunch-pair-integrated, rate of the T0 (top) and V0 (bottom) processes as a function of time, during the vdM scan session. The first (third) bell-shaped structure corresponds to the first (second) horizontal vdM scan. The second (fourth) bell-shaped structure corresponds to the first (second) vertical vdM scan. The fifth (sixth) bell-shaped structure corresponds to the horizontal (vertical) scan with a vertical (horizontal) offset. The two comb-shaped structures before the offset scans correspond to the horizontal and vertical length-scale calibration scans.

This procedure has only a small effect ($< 1\%$) when applied to the T0 rates, due to the vertex cut in the T0 trigger logic described in Sec. 2. In order to study a possible contamination of the trigger rate by the intrinsic noise counts of the detectors, the rate of both trigger signals in the absence of beam was measured and found to be zero. The rate in empty bunch slots with beam circulating was also measured and found to be zero for the T0. For the V0, a significant counting rate was measured in the slots immediately after a filled one, due to after-pulses. However, the rate in empty slots immediately preceding a filled one is smaller by a factor of about 10^{-5} than that in filled slots, pointing to a negligible after-pulse effect on the rate measurement. In addition, the probability of multiple interactions in the same bunch crossing (pileup) is taken into account according to Poisson statistics. Since both reference processes consist of a coincidence of hits on the A and C sides, their measured rate after background subtraction (R_{BB}) is given, for a given bunch pair, by

$$R_{\mathrm{BB}} = f_{\mathrm{rev}} \left\{1 - \exp\left(-\mu_{\mathrm{vis}}\right) + \exp\left(-\mu_{\mathrm{vis}}\right) \left[1 - \exp\left(-\mu_{\mathrm{AnotC}}\right)\right] \left[1 - \exp\left(-\mu_{\mathrm{CnotA}}\right)\right]\right\} \tag{3}$$

where $\mu_{\mathrm{vis}} = L\sigma_{\mathrm{vis}}/f_{\mathrm{rev}}$ is the average number of genuine coincidences (i.e. of visible interactions) per bunch crossing and μ_{AnotC} (μ_{CnotA}) is the average number of events per bunch crossing where only the A (C) side has an hit. The ratios $\alpha = \mu_{\mathrm{AnotC}}/\mu_{\mathrm{vis}}$ and $\beta = \mu_{\mathrm{CnotA}}/\mu_{\mathrm{vis}}$ were measured from data collected in low-pileup conditions ($\mu_{\mathrm{vis}} \simeq 0.005$ for the T0, $\simeq 0.01$ for the V0); for the T0 they amount to $\alpha = 0.44$, $\beta = 0.38$, for the V0 they amount to $\alpha = 0.079$, $\beta = 0.068$. These results have negligible statistical uncertainty and include a small ($\simeq$1%) correction for the non-zero μ_{vis} value at which they were measured. Knowledge of α and β allows one to retrieve the value of μ_{vis} from the measured R_{BB}, by numerically inverting equation 3. The pileup-free process rate is then given by $R_{\mathrm{PU}} = f_{\mathrm{rev}}\mu_{\mathrm{vis}}$. Finally, a correction is performed to account for the bunch intensity (and, hence, the luminosity) decay with time. The rates at each separation[3] are rescaled by the ratio of the corresponding bunch intensities to the bunch intensities at an arbitrary timestamp (t_0), chosen to lie between the horizontal and vertical scan. The relative modification of the rate after each of the three steps is shown, as a function of the beam separation, in Fig. 2.

The measured scan curves are also corrected for orbit drift and beam-beam deflections. Orbit drifts, i.e. variations in time of the reference beam orbit, may lead to a difference between the nominal and the actual beam separation. In order to quantify the bias, the data from the LHC Beam Position Monitors (BPM) [15] in various locations along the ring are used to extrapolate the transverse coordinates of the reference orbit of the two beams at IP2, for each scan step, using the YASP steering program [16]. Due to leakage of the (nominally closed) orbit bumps induced by the corrector magnets used for the vdM scan, the BPM data collected during the scan cannot be used for such a procedure, since they are themselves affected by the scan features. Hence, data was collected in between and outside scans, and their time-dependence was fitted with a polynomial function, which was then used to interpolate the reference orbit position of each beam during the scan, and to determine the correction to their separation. Due to their electric charge, the two beams exert a repulsive force upon each other [17]. Such a repulsion (beam-beam deflection) affects the beam separation. The corrections to the orbit-drift-corrected beam separation, which depend on the separation itself, on the bunch pair intensities, on the effective beam widths h_{x} and h_{y}[4], and on the accelerator optics parameters (betatron tunes Q_x and Q_y, β^*), were calculated using the MAD-X [18] code. An example of the obtained orbit-drift and beam-beam-deflection correction values as a function of the beam separation is shown in Fig. 3.

Once the corrections described above are applied, the scan curves are fitted, to determine the effective beam widths h_x and h_y. It was found that the scan curves $R(\Delta x, 0)$ and $R(0, \Delta y)$ are satisfactorily described

[3] The acquisition time for each separation value is 30 s, negligibile with respect to the half-life of the beam, which is typically of a few hours

[4] The beam widths used for this step are obtained from a preliminary analysis where orbit drift alone is taken into account. It was checked that such an approximation results in a negligible bias on the obtained deflection values.

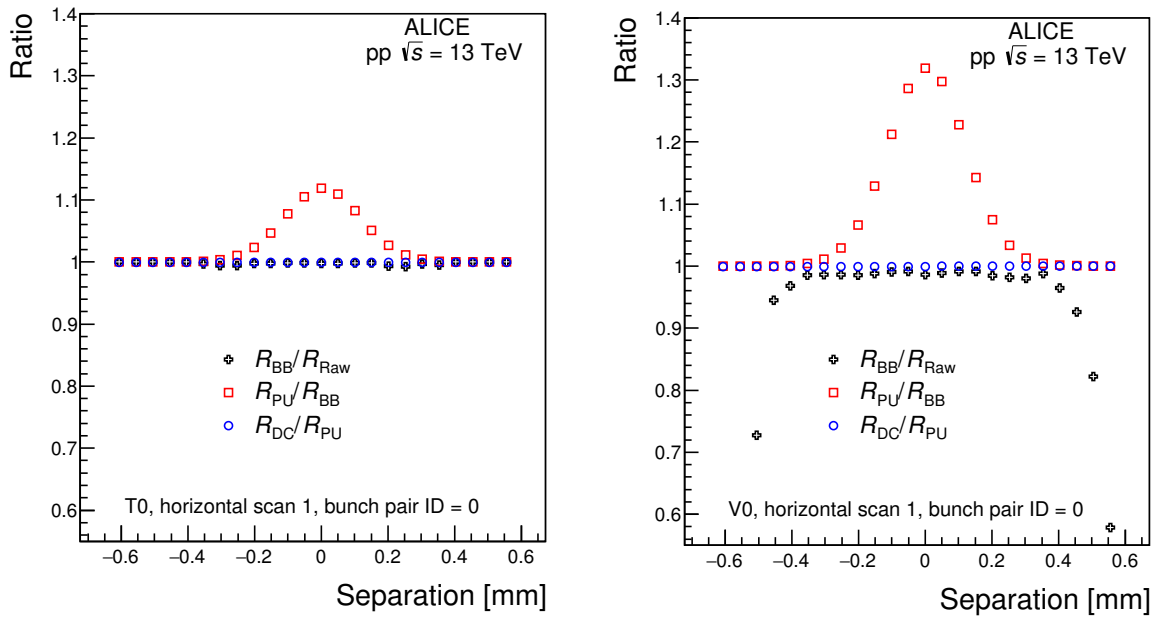

Fig. 2: (Colour online) Relative modification of the T0 (left) and V0 (right) trigger rate after background (R_{BB}/R_{raw}), pileup (R_{PU}/R_{BB}) and luminosity decay (R_{DC}/R_{PU}) are taken into account, as a function of the beam separation, for one typical pair of colliding bunches during the first horizontal scan.

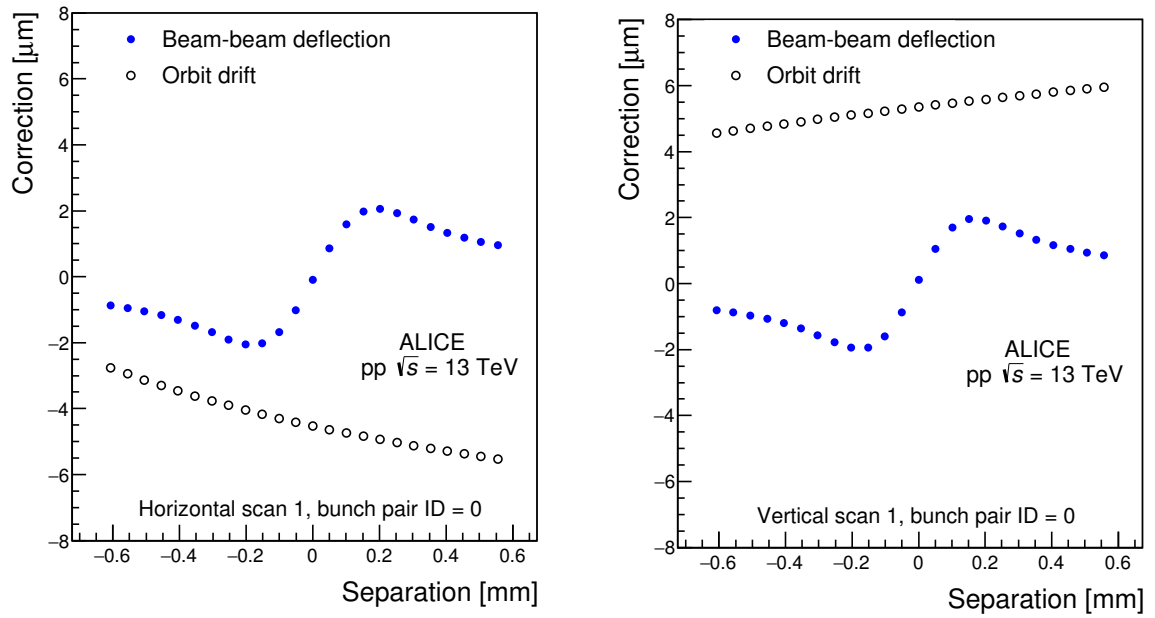

Fig. 3: (Colour online) Orbit-drift and beam-beam-deflection corrections to the beam separation during the first horizontal (left) and vertical (right) scan, for one typical pair of colliding bunches, as a function of the nominal separation.

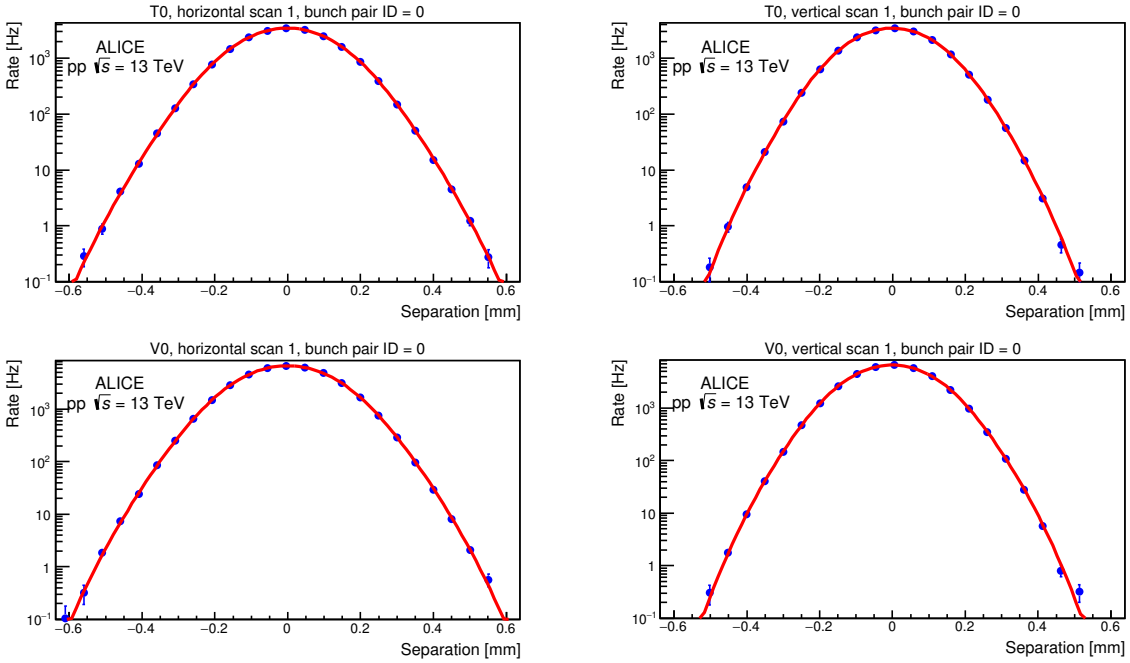

Fig. 4: (Colour online) Rates of the T0 (top) and V0 (bottom) reference processes as a function of beam separation for one typical pair of colliding bunches in the first horizontal (left) and vertical (right) vdM scan. The solid red curve is a fit according to eq. 4.

by a Gaussian function multiplied by a symmetric sixth-order polynomial function:

$$R(\Delta x,0) = R(0,0)\exp\left[-(\Delta x-\mu)^2/2\sigma^2\right]\left[1+p_2(\Delta x-\mu)^2+p_4(\Delta x-\mu)^4+p_6(\Delta x-\mu)^6\right], \quad (4)$$

and similarly for $R(0,\Delta y)$. $R(0,0)$, μ, σ, p_2, p_4 and p_6 are fit parameters. The χ^2/ndf value of the fit is $\simeq$1 on average, and typically below 3. As an example, the fitted curves for one bunch pair are shown in Fig. 4. Two more models were tested and used for systematic uncertainty evaluation (see Sec. 4). Since the effective beam widths are independent of the process used to measure them, a consistency check is performed by computing the ratio of the $h_x h_y$ quantities of equation 1 obtained with the T0 and the V0 for each colliding bunch. The results are shown in Fig. 5. The bunch-averaged value of the ratios is compatible with unity within 0.6%.

The measured beam widths are corrected by a length-scale calibration factor. This correction aims to fine tune the conversion factor (known with limited precision) between the current in the steering magnets and the beam displacement. The calibration is performed in a dedicated run, where the two beams are moved simultaneously in the same direction in steps of equal size; the changes in the primary interaction vertex position provide a measurement of the actual beam displacement, which is used to extract a correction factor to the nominal displacement scale. The vertex position is measured using tracks reconstructed in the ALICE Inner Tracking System [19] and Time Projection Chamber [20]. For each step, the vertex position and its uncertainty are obtained from a Gaussian fit to the vertex distribution. The length-scale correction factor is the slope parameter of a linear fit to the measured vertex displacement as a function of the nominal displacement (Fig. 6). Since this correction affects the global beam-displacement scale, all measured beam widths are multiplied by the correction factors 0.9964±0.0046 for the horizontal scale and 0.9952±0.0012 for the vertical scale. Note that, for the horizontal scan, the linear fit yields $\chi^2/ndf \simeq 9$; in order to account for this, the uncertainty on the slope factor has been recomputed after rescaling the uncertainty of each data point by $\sqrt{\chi^2/ndf}$.

The possible presence of non-factorisation effects is assessed using the method proposed in [21]. First,

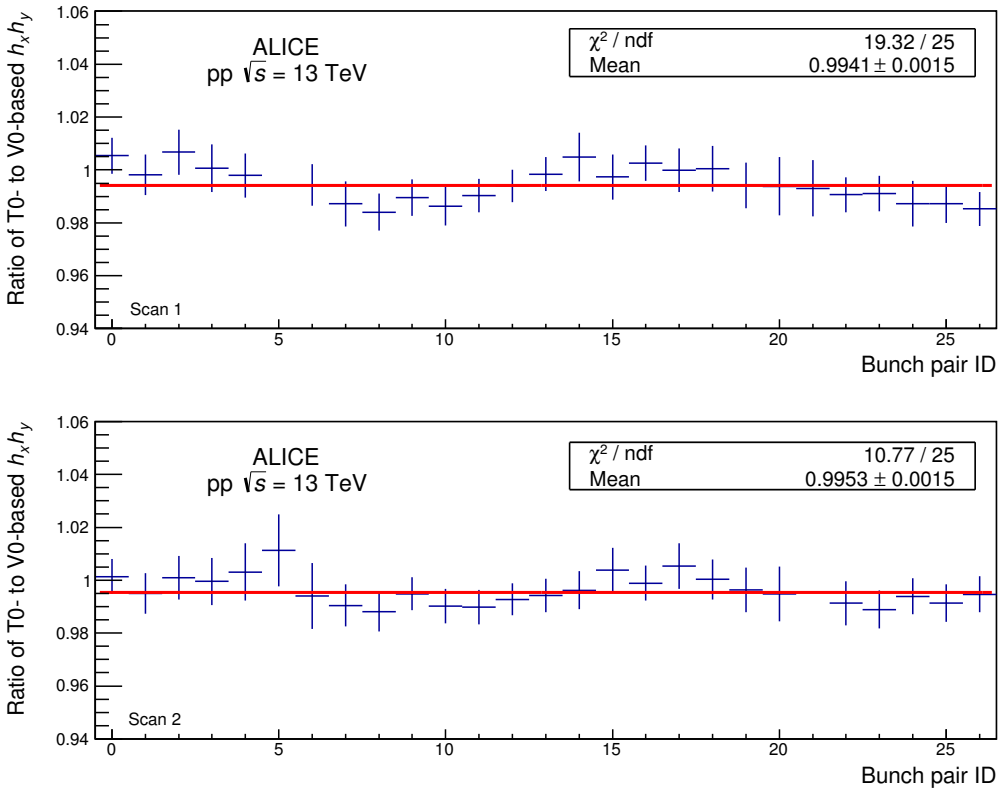

Fig. 5: (Colour online) Ratio between the $h_x h_y$ quantities obtained with the T0 and V0 reference processes in two vdM scans, as a function of the colliding bunch pair ID number. The solid red lines are zero-order-polynomial fits to the data.

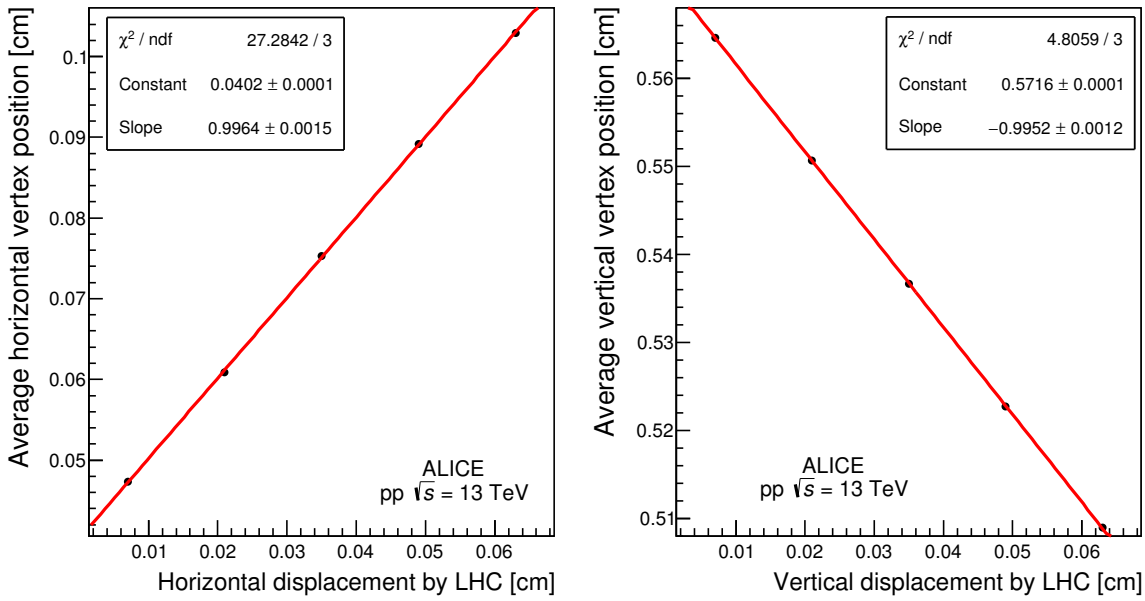

Fig. 6: (Colour online) Average horizontal (left) and vertical (right) vertex coordinate as a function of the nominal beam displacement in the length-scale calibration run, with superimposed linear fit (solid red line).

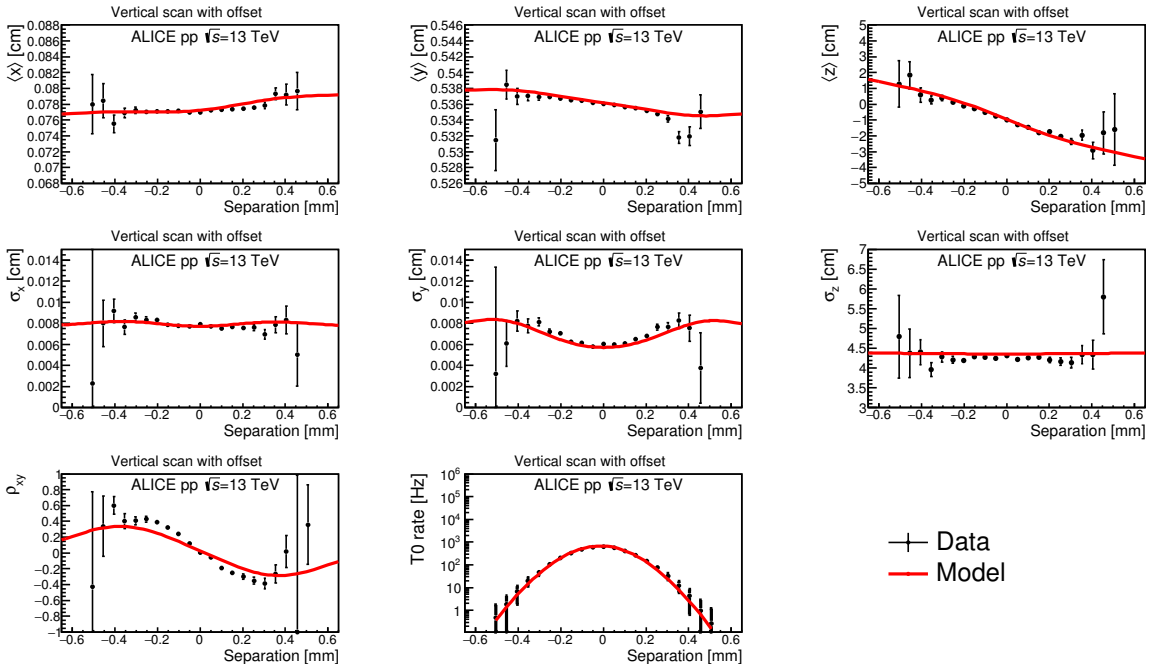

Fig. 7: (Colour online) Luminous region parameters and T0 rate as a function of separation during a vertical scan with a horizontal offset, as fitted by a three-dimensional correlated model [21] (solid red line). The centroids are shown in the top row, the RMS sizes are shown in the middle row, the transverse tilt is shown in the bottom row together with the T0 rate.

the three-dimensional vertex distribution is measured using the ITS and TPC, for each separation step during the standard and offset scans, and used to determine the beam spot position, its RMS size along the three spatial directions, and its transverse tilt (x-y covariance). Deconvolution of the finite detector resolution for vertex determination is performed with the method described in [22]. Second, the evolution of the beam spot parameters and reference process rates with separation is simultaneously fitted according to a model assuming that the probability density function of particles in a bunch is a three-dimensional non-factorisable double-Gaussian. Data from all scans are fitted together. As shown in Fig. 7 for one of the offset scans, the model is able to reproduce the main features of the evolution with separation of the luminous region parameters. Third, the obtained fit parameters are used to compute the luminosity for head-on beams, which is then compared to that obtained with equation 1. The resulting correction factor, integrated over all colliding bunch pairs, is 1.009 ± 0.002. It enters the analysis as a multiplicative factor to $\sigma_{\rm vis}$. Due to a dependence of dead-time effects on the bunch-pair position in the filling scheme, a statistically significant bunch-by-bunch measurement of the correction factor cannot be performed. It has however been checked that the results for those bunches for which the measurement is feasible are all compatible among themselves and with the integrated result.

The cross section for each colliding bunch pair and reference process is calculated according to eq. 1 and 2 from the measured bunch intensities, from the beam widths and head-on rates obtained from the fit to the scan curves, and applying the length-scale and non-factorisation corrections. As there are two measured head-on rates per scan pair (one from the vertical and one from the horizontal scan), the arithmetic mean of the two is used. The head-on rates measured during the horizontal and the vertical scan differ by at most 0.4%, such a difference not being compatible with the statistical uncertainty. The measured visible cross sections for the T0-based (V0-based) reference process in the two scans are shown in Fig. 8 (Fig. 9) for all the colliding bunch pairs[5], as a function of the product $N_1 N_2$ of the colliding bunch

[5] One out of the 27 colliding bunch pairs has been discarded, due to a non-converging fit.

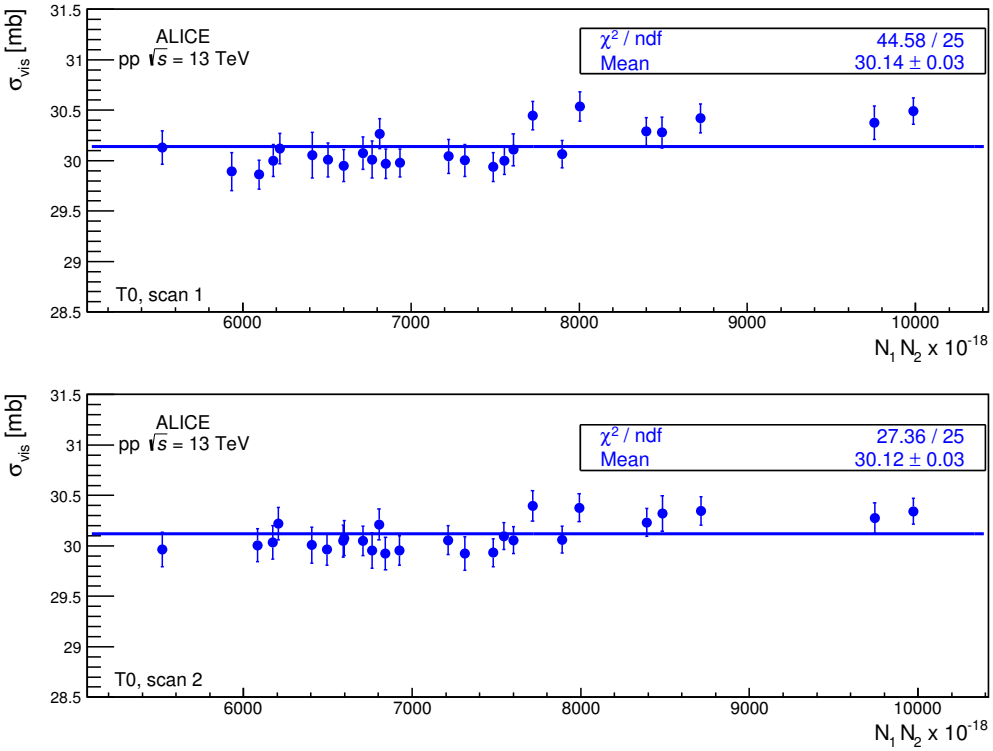

Fig. 8: Visible cross section for the T0 measured in the first (top) and second (bottom) vdM scan, as a function of the product of the intensities of the colliding bunch pair. Only the statistical uncertainties are shown. The solid line is a zero-order-polynomial fit to the data.

intensities. No strong dependence of the results on N_1N_2 is observed. For the first scan, fluctuations are slightly larger than justified by the statistical uncertainties, the χ^2/ndf value of a zero-order polynomial being 1.8; this observation is accounted for in the uncertainties (see Sec. 4).

4 vdM scan results

For both processes, and for the two scans, the weighted average of results from all colliding bunch pairs is computed (Fig.s 8 and 9). For the first scan, the average is performed after rescaling all the single-bunch uncertainties by a factor of $\sqrt{1.8}$, to account for the fluctuations mentioned at the end of Sec. 3. The weighted average of the results of the two scans is retained as the final result: σ_{T0} = 30.13 $\pm$ 0.02 $(stat.)$ mb, σ_{V0} = 57.77 $\pm$ 0.05 $(stat.)$ mb. Note that, if beam-beam deflection and orbit drifts had not been taken into account, the average cross sections would have been lower by 1.8%. The effect of orbit drift alone is 0.8%, in the same direction.

The sources of systematic uncertainty considered are listed below; unless otherwise specified, the quoted uncertainties apply to both the T0 and the V0 cross-section measurements.

– Non-factorisation: an uncertainty the same size as the applied correction (0.9%) is assigned to this effect.

– Orbit drift: an uncertainty the same size as the applied correction (0.8%) is assigned to this effect.

– Beam-beam deflection: the corrections to the beam separation have been recomputed after varying the optics parameters within their typical uncertainties ($\pm$ 0.02 units for the betatron tunes, $\pm$ 20%

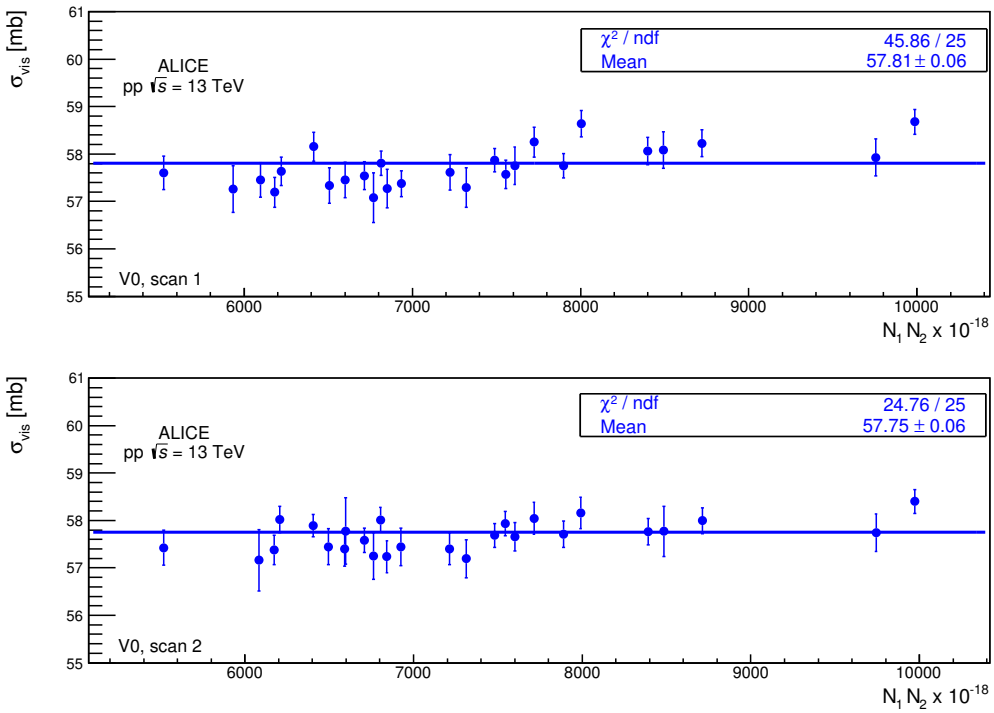

Fig. 9: Visible cross section for the V0 measured in the first (top) and second (bottom) vdM scan, as a function of the product of the intensities of the colliding bunch pair. Only the statistical uncertainties are shown. The solid line is a zero-order-polynomial fit to the data.

for β^*), and the beam widths within their statistical uncertainties. The resulting uncertainty on the cross section is 0.8%.

– Dynamic β^*: due to their electric charge, the two colliding beams (de-)focus each other in a separation-dependent way, which alters the measured scan shape. Calculations [23] are used to estimate the variations of β^* with the separation, according to the prescription given in [5]; the effect on the measured cross section is found to be 0.35% at most.

– Background subtraction: in order to evaluate a possible bias arising from beam-beam events identified as beam-gas by the cut described in Sec. 3, the analysis has been repeated by increasing the width of the window for beam-beam events from 6 to 12 ns: for the V0 (T0) cross section, a difference of 0.7% (0.1%) is found and added as a systematic uncertainty.

– Pileup: the analysis has been repeated by varying the α and β parameters (see Sec. 3) within a conservative 10% uncertainty. The effect on the cross section is at most 0.3% for the T0, and negligible ($\ll 0.1\%$) for the V0. The probability for accidental coincidences of noise counts on one detector arm and hits from pp collisions on the other arm was also evaluated, via the measured noise counting rate and the α and β parameters, and found to be negligible ($< 0.05\%$) for both luminometers. However, when comparing the ratio $\sigma_{\mathrm{T0}}/\sigma_{\mathrm{V0}}$ obtained from the vdM scan (where, for head-on beams, $\mu_{\mathrm{vis}} \simeq 0.4$-$0.7$ for the V0) to the ratio between the T0 and V0 rates measured at low interaction rate ($\mu_{\mathrm{vis}} \simeq 0.01$ for the V0) in the same LHC fill as the vdM scan, a difference of 0.9% is measured. To account for such a discrepancy of the ratio, an uncorrelated systematic uncertainty of 0.7% is assigned to both cross sections.

– Length-scale calibration: the quadratic sum of the uncertainties on the horizontal and vertical scale factors reported in Sec. 3 results in an uncertainty of 0.5%.

- Fit-model dependence: the analysis has been repeated by fitting the scan curve with a double-Gaussian function (which reproduces the data reasonably well, although with slightly larger residuals than found for the modified Gaussian function of equation 4), and by using numerical integration of the scan curve (see reference [14] for details) instead of a fit. The typical observed deviation with respect to the results of the standard method is 0.6%.
- Consistency of the measured beam widths: 0.6%, from the bunch-pair-averaged difference between the $h_x h_y$ quantities measured with the T0 and the V0 (Fig. 5).
- Luminosity decay: the bias arising from the variations in time of the head-on luminosity (expected from intensity burn-off, emittance growth and, possibly, a residual orbit-drift effect) is estimated via the difference (0.4%) between the head-on rates measured in the horizontal and vertical scans.
- Bunch-by-bunch consistency: the effect of rescaling the single-bunch statistical uncertainties to account for fluctuations in the first scan is equivalent to adding an additional uncertainty of 0.04% to the statistical uncertainty of the scan-averaged cross section.
- Scan-to-scan consistency: for both the T0 and the V0, the difference between the bunch-pair-averaged results from the two scans is $< 0.1\%$, and compatible with the statistical uncertainties.
- Beam centreing: the measurement of $R(0,0)$ can be affected by a non-optimal alignment of the two beams in the head-on position. Such a misalignment is quantified, for the x and y directions, via the μ parameter of eq. 4. The maximum observed misalignment is about 2 μm; its effect on the measured head-on rates was estimated using eq. 4 and the obtained fit parameters, and found to be negligible ($< 0.1\%$).
- Bunch intensity: the uncertainty on the bunch-intensity product $N_1 N_2$ has three components: the uncertainty of 0.3% on the absolute DCCT calibration, evaluated as outlined in [24]; the uncertainty (negligible, see Sec. 2) on the ghost and satellite charge; the uncertainty, of 0.5%, resulting from the relative bunch populations, evaluated by using a second device [25] for their measurement. Combining these three sources results in a total uncertainty of 0.6%.

Combining all the above-mentioned uncertainties, one obtains a total systematic uncertainty of about 2.1%, with an uncorrelated component between the two measurements arising from pileup and background subtraction.

The results for the visible cross sections are then

$$\sigma_{\mathrm{T0}} = (30.1 \pm 0.6)\,\mathrm{mb}\,, \quad \sigma_{\mathrm{V0}} = (57.8 \pm 1.2)\,\mathrm{mb},$$

where the uncertainties are systematic.

5 Consistency and stability of the vdM-based calibration

In order to test the stability of the luminosity measurement provided by the T0 and the V0, the ratio between their trigger rates in pp collisions at $\sqrt{s}$ = 13 TeV has been computed, for all runs[6] recorded in 2015. During the first month of data taking, the LHC filling schemes had large spacing between consecutive bunches (isolated bunches); then, denser filling schemes were used, with the bunches injected in trains with a spacing between bunches in a same train of 50 ns at first and 25 ns later in the year. In the period with isolated bunches, ALICE took data at $\mu_{\mathrm{vis}} \simeq 0.001$-$0.1$; with 50-ns-spaced trains, at $\mu_{\mathrm{vis}} \simeq 0.1$-$1$; with 25-ns-spaced trains, at $\mu_{\mathrm{vis}} \simeq 0.001$-$0.01$, where all μ_{vis} values refer to the V0.

[6] In the ALICE nomenclature, a run is a set of data collected within a start and a stop of the data acquisition, under stable detector and trigger configuration.

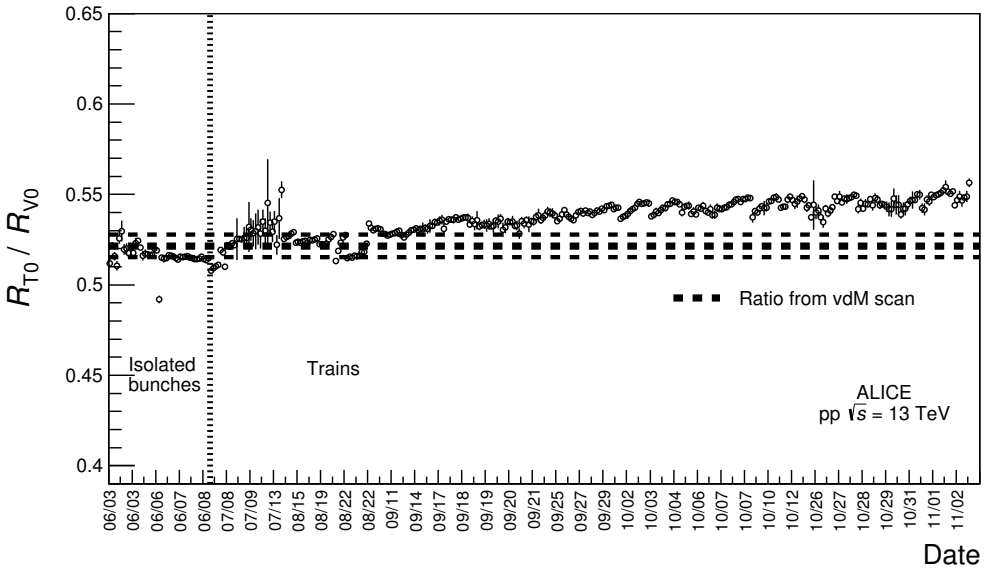

Fig. 10: Time-dependence of the ratio of the T0 rate to that of the V0, throughout the whole 2015 running period. The central horizontal dashed line indicates the expected ratio from the vdM scan, the upper and lower lines define its uncertainty band. The dotted vertical line marks the beginning of data-taking with bunch trains (see text for details).

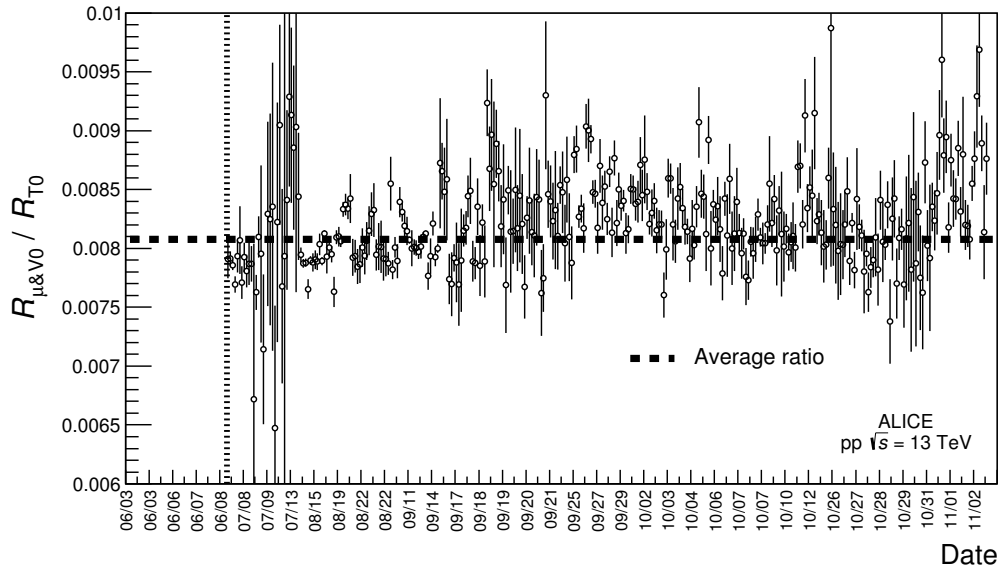

Fig. 11: Time-dependence of the ratio of the μ&V0 rate to that of the T0, throughout the whole 2015 running period. The horizontal dashed line indicates the average value of the ratio. The dotted vertical line marks the beginning of data-taking with bunch trains (see text for details).

The reference process rates are determined from the raw rates with the same procedure used in the vdM scan and described in Sec. 3. In order to suppress the bias induced by after-pulses on the V0 rates for dense filling schemes, the raw rates are measured after the data-acquisition system veto and corrected by the trigger dead-time. The results are shown as a function of time in Fig. 10. During the period with isolated bunches (and relatively small $\mu_{\rm vis}$), the ratio is reasonably stable. Its average value is smaller than expected from the vdM scan results by about 1%, but still compatible with it within the uncorrelated uncertainties of the two cross section measurements (see Sec. 4). For these running conditions, an additional uncertainty of 0.6% (corresponding to the RMS of the ratio distribution over the period) is assigned to the luminosity measurement. During data-taking with trains, relatively large fluctuations are observed as well as a constantly increasing trend. The trend can be understood as due to ageing of the V0 photomultipliers, causing loss of trigger efficiency for low-multiplicity events. Such a hypothesis was verified by comparing the V0 signal amplitude distributions at different moments during the year. The fluctuations may be explained by a number of effects, including: a filling-scheme dependence of the V0 efficiency due to pulse-length effects, particularly for 25-ns-spaced schemes; a degradation of the V0 timing resolution at relatively high $\mu_{\rm vis}$, affecting the cuts used for background subtraction; and possibly a run-dependent contamination from pile-up effects involving beam-gas hits at low $\mu_{\rm vis}$, potentially affecting both luminometers. It is concluded from all the above that, in case of LHC operation with trains, a luminosity measurement with the V0 is affected by non-trivial systematics requiring further studies, and the T0 is chosen as the preferred luminometer for such a running mode. In an attempt to assess the stability of the T0 in an unbiased manner, a second reference signal (μ&V0) was built by requiring, on top of the V0-based trigger, the detection of a muon with transverse momentum $p_{\rm T} > 1$ GeV/c (and $-4 < \eta < -2.5$) by the muon trigger system [26]. Such a trigger signal is expected to be less sensitive to ageing effects in the V0 (since the muon requirement biases the trigger event selection towards higher multiplicities). The ratio between the two trigger signals is shown as a function of time in Fig. 11. The overall trend seems to be mitigated, although with relatively large statistical uncertainties; some fluctuations are observed. The RMS of the ratio distribution, after subtraction of the statistical component, is 2.7%: this value is assigned as an additional systematic uncertainty on the T0-based luminosity measurement.

6 Conclusions

In August 2015, a vdM scan was performed in pp collisions at $\sqrt{s}$ = 13 TeV. Visible cross sections were measured for two reference processes, based on the T0 (with pseudorapidity coverage $4.6 < \eta < 4.9$, $-3.3 < \eta < -3.0$) and V0 ($2.8 < \eta < 5.1$, $-3.7 < \eta < -1.7$) detectors. The stability and consistency of the luminosity measurements based on such visible cross sections have been studied for the full data sample collected in 2015. A detailed list of the origin and size of the considered uncertainties for both the visible cross section and the luminosity measurement is reported in Table 5. When the LHC is operated with isolated-bunch-based filling schemes, the two detectors provide independent measurements of the luminosity, with a total uncertainty of 2.3%. When the LHC is operated with bunch trains the V0-based luminosity is affected by non-trivial systematic effects; in this case, the total uncertainty on the luminosity, measured with T0, is 3.4%.

Acknowledgements

The ALICE Collaboration would like to thank all its engineers and technicians for their invaluable contributions to the construction of the experiment and the CERN accelerator teams for the outstanding performance of the LHC complex. The ALICE Collaboration gratefully acknowledges the resources and support provided by all Grid centres and the Worldwide LHC Computing Grid (WLCG) collaboration. The ALICE Collaboration acknowledges the following funding agencies for their support in building and running the ALICE detector: State Committee of Science, World Federation of Scientists (WFS)

Source	Uncertainty
Non-factorisation	0.9%
Orbit drift	0.8%
Beam-beam deflection	0.8%
Dynamic β^*	0.3%
Background subtraction	0.1% (T0), 0.7% (V0)
Pileup	0.7%
Length-scale calibration	0.5%
Fit model	0.6%
$h_x h_y$ consistency (T0 vs V0)	0.6%
Luminosity decay	0.4%
Bunch-by-bunch consistency	< 0.1%
Scan-to-scan consistency	< 0.1%
Beam centreing	< 0.1%
Bunch intensity	0.6%
Total on visible cross section	2.05% (T0), 2.16% (V0)
Stability and consistency	0.6% (isolated bunches) 2.7% (whole 2015)
Total on luminosity	2.2% (isolated bunches) 3.4% (whole 2015)

Table 1: Relative uncertainties on the measurement of visible cross sections and luminosity in pp collisions at $\sqrt{s}$ = 13 TeV.

and Swiss Fonds Kidagan, Armenia; Conselho Nacional de Desenvolvimento Científico e Tecnológico (CNPq), Financiadora de Estudos e Projetos (FINEP), Fundação de Amparo à Pesquisa do Estado de São Paulo (FAPESP); Ministry of Science & Technology of China (MSTC), National Natural Science Foundation of China (NSFC) and Ministry of Education of China (MOEC)"; Ministry of Science, Education and Sports of Croatia and Unity through Knowledge Fund, Croatia; Ministry of Education and Youth of the Czech Republic; Danish Natural Science Research Council, the Carlsberg Foundation and the Danish National Research Foundation; The European Research Council under the European Community's Seventh Framework Programme; Helsinki Institute of Physics and the Academy of Finland; French CNRS-IN2P3, the 'Region Pays de Loire', 'Region Alsace', 'Region Auvergne' and CEA, France; German Bundesministerium fur Bildung, Wissenschaft, Forschung und Technologie (BMBF) and the Helmholtz Association; General Secretariat for Research and Technology, Ministry of Development, Greece; National Research, Development and Innovation Office (NKFIH), Hungary; Council of Scientific and Industrial Research (CSIR), New Delhi; Department of Atomic Energy and Department of Science and Technology of the Government of India; Istituto Nazionale di Fisica Nucleare (INFN) and Centro Fermi - Museo Storico della Fisica e Centro Studi e Ricerche "Enrico Fermi", Italy; Japan Society for the Promotion of Science (JSPS) KAKENHI and MEXT, Japan; National Research Foundation of Korea (NRF); Consejo Nacional de Cienca y Tecnologia (CONACYT), Direccion General de Asuntos del Personal Academico(DGAPA), México, Amerique Latine Formation academique - European Commission (ALFA-EC) and the EPLANET Program (European Particle Physics Latin American Network); Stichting voor Fundamenteel Onderzoek der Materie (FOM) and the Nederlandse Organisatie voor Wetenschappelijk Onderzoek (NWO), Netherlands; Research Council of Norway (NFR); Pontificia Universidad Católica del Perú; National Science Centre, Poland; Ministry of National Education/Institute for Atomic Physics and National Council of Scientific Research in Higher Education (CNCSI-UEFISCDI), Romania; Joint Institute for Nuclear Research, Dubna; Ministry of Education and Science of Russian Federation, Russian Academy of Sciences, Russian Federal Agency of Atomic Energy, Russian Federal Agency for Science

and Innovations and The Russian Foundation for Basic Research; Ministry of Education of Slovakia; Department of Science and Technology, South Africa; Centro de Investigaciones Energeticas, Medioambientales y Tecnologicas (CIEMAT), E-Infrastructure shared between Europe and Latin America (EELA), Ministerio de Economía y Competitividad (MINECO) of Spain, Xunta de Galicia (Consellería de Educación), Centro de Aplicaciones Tecnológicas y Desarrollo Nuclear (CEADEN), Cubaenergía, Cuba, and IAEA (International Atomic Energy Agency); Swedish Research Council (VR) and Knut & Alice Wallenberg Foundation (KAW); National Science and Technology Development Agency (NSDTA), Suranaree University of Technology (SUT) and Office of the Higher Education Commission under NRU project of Thailand; Ukraine Ministry of Education and Science; United Kingdom Science and Technology Facilities Council (STFC); The United States Department of Energy, the United States National Science Foundation, the State of Texas, and the State of Ohio.

References

[1] **ALICE** Collaboration, K. Aamodt *et al.*, "The ALICE experiment at the CERN LHC," *JINST* **3** (2008) S08002.

[2] S. van der Meer, "Calibration of the effective beam height in the ISR," Tech. Rep. CERN-ISR-PO-68-31, CERN, 1968. http://cds.cern.ch/record/296752.

[3] V. Balagura, "Notes on van der Meer Scan for Absolute Luminosity Measurement," *Nucl. Instrum. Meth.* **A654** (2011) 634–638, arXiv:1103.1129 [physics.ins-det].

[4] **LHCb** Collaboration, R. Aaij *et al.*, "Precision luminosity measurements at LHCb," *JINST* **9** no. 12, (2014) P12005, arXiv:1410.0149 [hep-ex].

[5] **ATLAS** Collaboration, G. Aad *et al.*, "Improved luminosity determination in pp collisions at $\sqrt{s}$ = 7 TeV using the ATLAS detector at the LHC," *Eur. Phys. J.* **C73** no. 8, (2013) 2518, arXiv:1302.4393 [hep-ex].

[6] **CMS** Collaboration, "CMS Luminosity Based on Pixel Cluster Counting - Summer 2013 Update," Tech. Rep. CMS-PAS-LUM-13-001, CERN, 2013. https://cds.cern.ch/record/1598864.

[7] **ALICE** Collaboration, B. B. Abelev *et al.*, "Performance of the ALICE Experiment at the CERN LHC," *Int. J. Mod. Phys.* **A29** (2014) 1430044, arXiv:1402.4476 [nucl-ex].

[8] **ALICE T0 and V0** Collaboration, T. Malkiewicz *et al.*, "Luminosity determination in ALICE with T0 and V0 detectors," *Indian J. Phys.* **85** (2011) 965–970.

[9] **ALICE** Collaboration, E. Abbas *et al.*, "Performance of the ALICE VZERO system," *JINST* **8** (2013) P10016, arXiv:1306.3130 [nucl-ex].

[10] J. J. Gras, D. Belohrad, M. Ludwig, P. Odier, and C. Barschel, "Optimization of the LHC beam current transformers for accurate luminosity determination," Tech. Rep. CERN-ATS-2011-063, CERN, 2011. http://cds.cern.ch/record/1379466.

[11] A. Alici *et al.*, "Study of the LHC ghost charge and satellite bunches for luminosity calibration.," Tech. Rep. CERN-ATS-Note-2012-029 PERF, CERN, 2012. https://cds.cern.ch/record/1427728.

[12] C. Barschel, *Precision luminosity measurement at LHCb with beam-gas imaging*. PhD thesis, RWTH Aachen U., 2014. https://inspirehep.net/record/1339684/files/CERN-THESIS-2013-301.pdf.

[13] A. Boccardi, E. Bravin, M. Ferro-Luzzi, S. Mazzoni, and M. Palm, "LHC Luminosity calibration using the Longitudinal Density Monitor," Tech. Rep. CERN-ATS-Note-2013-034 TECH, CERN, 2013. https://cds.cern.ch/record/1556087.

[14] **ALICE** Collaboration, B. B. Abelev *et al.*, "Measurement of visible cross sections in proton-lead collisions at $\sqrt{s_{\rm NN}}$ = 5.02 TeV in van der Meer scans with the ALICE detector," *JINST* **9** no. 11, (2014) P11003, arXiv:1405.1849 [nucl-ex].

[15] D. Bishop, C. Boccard, E. Calvo-Giraldo, D. Cocq, L. Jensen, R. Jones, J. J. Savioz, and G. Waters, "The LHC Orbit and Trajectory System,". https://cds.cern.ch/record/624190.

[16] J. Wenninger, "Dispersion Free Steering for YASP and dispersion correction for TI8," Tech. Rep. LHC-Performance-Note-005, CERN, 2009. http://cds.cern.ch/record/1156142.

[17] W. Kozanecki, T. Pieloni, and J. Wenninger, "Observation of Beam-beam Deflections with LHC Orbit Data," Tech. Rep. CERN-ACC-NOTE-2013-0006, CERN, 2013. https://cds.cern.ch/record/1581723.

[18] CERN Accelerator Beam Physics Group, "MAD-Methodical Accelerator Design,". http://mad.web.cern.ch/mad/.

[19] **ALICE** Collaboration, K. Aamodt *et al.*, "Alignment of the ALICE Inner Tracking System with cosmic-ray tracks," *JINST* **5** (2010) P03003, arXiv:1001.0502 [physics.ins-det].

[20] J. Alme *et al.*, "The ALICE TPC, a large 3-dimensional tracking device with fast readout for ultra-high multiplicity events," *Nucl. Instrum. Meth.* **A622** (2010) 316–367, arXiv:1001.1950 [physics.ins-det].

[21] S. N. Webb, *Factorisation of beams in van der Meer scans and measurements of the ϕ^*_η distribution of $Z \to e^+e^-$ events in pp collisions at $\sqrt{s} = 8$ TeV with the ATLAS detector*. PhD thesis, Manchester U., 2015-06-01. https://inspirehep.net/record/1381312/files/CERN-THESIS-2015-054.pdf.

[22] **ATLAS** Collaboration, "Characterization of Interaction-Point Beam Parameters Using the pp Event-Vertex Distribution Reconstructed in the ATLAS Detector at the LHC," Tech. Rep. ATLAS-CONF-2010-027, CERN, 2010. https://cds.cern.ch/record/1277659.

[23] W. Herr, "Beam-beam effects and dynamic β^*," Tech. Rep. LHC Lumi Days 2012, CERN, 2012. https://indico.cern.ch/event/162948/.

[24] C. Barschel, M. Ferro-Luzzi, J.-J. Gras, M. Ludwig, P. Odier, and S. Thoulet, "Results of the LHC DCCT Calibration Studies," Tech. Rep. CERN-ATS-Note-2012-026 PERF, CERN, 2012. https://cds.cern.ch/record/1425904.

[25] C. Ohm and T. Pauly, "The ATLAS beam pick-up based timing system," *Nucl. Instrum. Meth.* **A623** (2010) 558–560, arXiv:0905.3648 [physics.ins-det].

[26] R. Arnaldi *et al.*, "Design and performance of the ALICE muon trigger system," *Nucl. Phys. Proc. Suppl.* **158** (2006) 21–24.

A The ALICE Collaboration

J. Adam[40], D. Adamová[86], M.M. Aggarwal[90], G. Aglieri Rinella[36], M. Agnello[31,112], N. Agrawal[49], Z. Ahammed[135], S. Ahmad[18], S.U. Ahn[70], S. Aiola[139], A. Akindinov[56], S.N. Alam[135], D.S.D. Albuquerque[123], D. Aleksandrov[82], B. Alessandro[112], D. Alexandre[103], R. Alfaro Molina[65], A. Alici[12,106], A. Alkin[3], J. Alme[22,38], T. Alt[43], S. Altinpinar[22], I. Altsybeev[134], C. Alves Garcia Prado[122], M. An[7], C. Andrei[80], H.A. Andrews[103], A. Andronic[99], V. Anguelov[95], T. Antičić[100], F. Antinori[109], P. Antonioli[106], L. Aphecetche[115], H. Appelshäuser[62], S. Arcelli[27], R. Arnaldi[112], O.W. Arnold[37,96], I.C. Arsene[21], M. Arslandok[62], B. Audurier[115], A. Augustinus[36], R. Averbeck[99], M.D. Azmi[18], A. Badalà[108], Y.W. Baek[69], S. Bagnasco[112], R. Bailhache[62], R. Bala[93], S. Balasubramanian[139], A. Baldisseri[15], R.C. Baral[59], A.M. Barbano[26], R. Barbera[28], F. Barile[33], G.G. Barnaföldi[138], L.S. Barnby[36,103], V. Barret[72], P. Bartalini[7], K. Barth[36], J. Bartke[I,119], E. Bartsch[62], M. Basile[27], N. Bastid[72], S. Basu[135], B. Bathen[63], G. Batigne[115], A. Batista Camejo[72], B. Batyunya[68], P.C. Batzing[21], I.G. Bearden[83], H. Beck[62,95], C. Bedda[112], N.K. Behera[52], I. Belikov[66], F. Bellini[27], H. Bello Martinez[2], R. Bellwied[124], R. Belmont[137], E. Belmont-Moreno[65], L.G.E. Beltran[121], V. Belyaev[77], G. Bencedi[138], S. Beole[26], I. Berceanu[80], A. Bercuci[80], Y. Berdnikov[88], D. Berenyi[138], R.A. Bertens[55], D. Berzano[36], L. Betev[36], A. Bhasin[93], I.R. Bhat[93], A.K. Bhati[90], B. Bhattacharjee[45], J. Bhom[119], L. Bianchi[124], N. Bianchi[74], C. Bianchin[137], J. Bielčík[40], J. Bielčíková[86], A. Bilandzic[37,83,96], G. Biro[138], R. Biswas[4], S. Biswas[4,81], S. Bjelogrlic[55], J.T. Blair[120], D. Blau[82], C. Blume[62], F. Bock[76,95], A. Bogdanov[77], H. Bøggild[83], L. Boldizsár[138], M. Bombara[41], M. Bonora[36], J. Book[62], H. Borel[15], A. Borissov[98], M. Borri[85,126], F. Bossú[67], E. Botta[26], C. Bourjau[83], P. Braun-Munzinger[99], M. Bregant[122], T. Breitner[61], T.A. Broker[62], T.A. Browning[97], M. Broz[40], E.J. Brucken[47], E. Bruna[112], G.E. Bruno[33], D. Budnikov[101], H. Buesching[62], S. Bufalino[26,31], P. Buncic[36], O. Busch[130], Z. Buthelezi[67], J.B. Butt[16], J.T. Buxton[19], J. Cabala[117], D. Caffarri[36], X. Cai[7], H. Caines[139], L. Calero Diaz[74], A. Caliva[55], E. Calvo Villar[104], P. Camerini[25], F. Carena[36], W. Carena[36], F. Carnesecchi[27], J. Castillo Castellanos[15], A.J. Castro[127], E.A.R. Casula[24], C. Ceballos Sanchez[9], J. Cepila[40], P. Cerello[112], J. Cerkala[117], B. Chang[125], S. Chapeland[36], M. Chartier[126], J.L. Charvet[15], S. Chattopadhyay[135], S. Chattopadhyay[102], A. Chauvin[37,96], V. Chelnokov[3], M. Cherney[89], C. Cheshkov[132], B. Cheynis[132], V. Chibante Barroso[36], D.D. Chinellato[123], S. Cho[52], P. Chochula[36], K. Choi[98], M. Chojnacki[83], S. Choudhury[135], P. Christakoglou[84], C.H. Christensen[83], P. Christiansen[34], T. Chujo[130], S.U. Chung[98], C. Cicalo[107], L. Cifarelli[12,27], F. Cindolo[106], J. Cleymans[92], F. Colamaria[33], D. Colella[36,57], A. Collu[76], M. Colocci[27], G. Conesa Balbastre[73], Z. Conesa del Valle[53], M.E. Connors[II,139], J.G. Contreras[40], T.M. Cormier[87], Y. Corrales Morales[26,112], I. Cortés Maldonado[2], P. Cortese[32], M.R. Cosentino[122], F. Costa[36], J. Crkovska[53], P. Crochet[72], R. Cruz Albino[11], E. Cuautle[64], L. Cunqueiro[36,63], T. Dahms[37,96], A. Dainese[109], M.C. Danisch[95], A. Danu[60], D. Das[102], I. Das[102], S. Das[4], A. Dash[81], S. Dash[49], S. De[122], A. De Caro[30], G. de Cataldo[105], C. de Conti[122], J. de Cuveland[43], A. De Falco[24], D. De Gruttola[12,30], N. De Marco[112], S. De Pasquale[30], R.D. De Souza[123], A. Deisting[95,99], A. Deloff[79], C. Deplano[84], P. Dhankher[49], D. Di Bari[33], A. Di Mauro[36], P. Di Nezza[74], B. Di Ruzza[109], M.A. Diaz Corchero[10], T. Dietel[92], P. Dillenseger[62], R. Divià[36], Ø. Djuvsland[22], A. Dobrin[60,84], D. Domenicis Gimenez[122], B. Dönigus[62], O. Dordic[21], T. Drozhzhova[62], A.K. Dubey[135], A. Dubla[55], L. Ducroux[132], P. Dupieux[72], R.J. Ehlers[139], D. Elia[105], E. Endress[104], H. Engel[61], E. Epple[139], B. Erazmus[115], I. Erdemir[62], F. Erhardt[131], B. Espagnon[53], M. Estienne[115], S. Esumi[130], G. Eulisse[36], J. Eum[98], D. Evans[103], S. Evdokimov[113], G. Eyyubova[40], L. Fabbietti[37,96], D. Fabris[109], J. Faivre[73], A. Fantoni[74], M. Fasel[76], L. Feldkamp[63], A. Feliciello[112], G. Feofilov[134], J. Ferencei[86], A. Fernández Téllez[2], E.G. Ferreiro[17], A. Ferretti[26], A. Festanti[29], V.J.G. Feuillard[15,72], J. Figiel[119], M.A.S. Figueredo[122], S. Filchagin[101], D. Finogeev[54], F.M. Fionda[24], E.M. Fiore[33], M. Floris[36], S. Foertsch[67], P. Foka[99], S. Fokin[82], E. Fragiacomo[111], A. Francescon[36], A. Francisco[115], U. Frankenfeld[99], G.G. Fronze[26], U. Fuchs[36], C. Furget[73], A. Furs[54], M. Fusco Girard[30], J.J. Gaardhøje[83], M. Gagliardi[26], A.M. Gago[104], K. Gajdosova[83], M. Gallio[26], C.D. Galvan[121], D.R. Gangadharan[76], P. Ganoti[91], C. Gao[7], C. Garabatos[99], E. Garcia-Solis[13], K. Garg[28], C. Gargiulo[36], P. Gasik[37,96], E.F. Gauger[120], M. Germain[115], M. Gheata[36,60], P. Ghosh[135], S.K. Ghosh[4], P. Gianotti[74], P. Giubellino[36,112], P. Giubilato[29], E. Gladysz-Dziadus[119], P. Glässel[95], D.M. Goméz Coral[65], A. Gomez Ramirez[61], A.S. Gonzalez[36], V. Gonzalez[10], P. González-Zamora[10], S. Gorbunov[43], L. Görlich[119], S. Gotovac[118], V. Grabski[65], O.A. Grachov[139],

L.K. Graczykowski[136], K.L. Graham[103], A. Grelli[55], A. Grigoras[36], C. Grigoras[36], V. Grigoriev[77], A. Grigoryan[1], S. Grigoryan[68], B. Grinyov[3], N. Grion[111], J.M. Gronefeld[99], J.F. Grosse-Oetringhaus[36], R. Grosso[99], L. Gruber[114], F. Guber[54], R. Guernane[73], B. Guerzoni[27], K. Gulbrandsen[83], T. Gunji[129], A. Gupta[93], R. Gupta[93], I.B. Guzman[2], R. Haake[36,63], C. Hadjidakis[53], M. Haiduc[60], H. Hamagaki[129], G. Hamar[138], J.C. Hamon[66], J.W. Harris[139], A. Harton[13], D. Hatzifotiadou[106], S. Hayashi[129], S.T. Heckel[62], E. Hellbär[62], H. Helstrup[38], A. Herghelegiu[80], G. Herrera Corral[11], F. Herrmann[63], B.A. Hess[35], K.F. Hetland[38], H. Hillemanns[36], B. Hippolyte[66], D. Horak[40], R. Hosokawa[130], P. Hristov[36], C. Hughes[127], T.J. Humanic[19], N. Hussain[45], T. Hussain[18], D. Hutter[43], D.S. Hwang[20], R. Ilkaev[101], M. Inaba[130], E. Incani[24], M. Ippolitov[77,82], M. Irfan[18], V. Isakov[54], M. Ivanov[36,99], V. Ivanov[88], V. Izucheev[113], B. Jacak[76], N. Jacazio[27], P.M. Jacobs[76], M.B. Jadhav[49], S. Jadlovska[117], J. Jadlovsky[57,117], C. Jahnke[37,122], M.J. Jakubowska[136], M.A. Janik[136], P.H.S.Y. Jayarathna[124], C. Jena[29], S. Jena[124], R.T. Jimenez Bustamante[99], P.G. Jones[103], H. Jung[44], A. Jusko[103], P. Kalinak[57], A. Kalweit[36], J.H. Kang[140], V. Kaplin[77], S. Kar[135], A. Karasu Uysal[71], O. Karavichev[54], T. Karavicheva[54], L. Karayan[95,99], E. Karpechev[54], U. Kebschull[61], R. Keidel[141], D.L.D. Keijdener[55], M. Keil[36], M. Mohisin Khan[III,18], P. Khan[102], S.A. Khan[135], A. Khanzadeev[88], Y. Kharlov[113], A. Khatun[18], B. Kileng[38], D.W. Kim[44], D.J. Kim[125], D. Kim[140], H. Kim[140], J.S. Kim[44], J. Kim[95], M. Kim[140], S. Kim[20], T. Kim[140], S. Kirsch[43], I. Kisel[43], S. Kiselev[56], A. Kisiel[136], G. Kiss[138], J.L. Klay[6], C. Klein[62], J. Klein[36], C. Klein-Bösing[63], S. Klewin[95], A. Kluge[36], M.L. Knichel[95], A.G. Knospe[120,124], C. Kobdaj[116], M. Kofarago[36], T. Kollegger[99], A. Kolojvari[134], V. Kondratiev[134], N. Kondratyeva[77], E. Kondratyuk[113], A. Konevskikh[54], M. Kopcik[117], M. Kour[93], C. Kouzinopoulos[36], O. Kovalenko[79], V. Kovalenko[134], M. Kowalski[119], G. Koyithatta Meethaleveedu[49], I. Králik[57], A. Kravčáková[41], M. Krivda[57,103], F. Krizek[86], E. Kryshen[36,88], M. Krzewicki[43], A.M. Kubera[19], V. Kučera[86], C. Kuhn[66], P.G. Kuijer[84], A. Kumar[93], J. Kumar[49], L. Kumar[90], S. Kumar[49], P. Kurashvili[79], A. Kurepin[54], A.B. Kurepin[54], A. Kuryakin[101], M.J. Kweon[52], Y. Kwon[140], S.L. La Pointe[43,112], P. La Rocca[28], P. Ladron de Guevara[11], C. Lagana Fernandes[122], I. Lakomov[36], R. Langoy[42], K. Lapidus[37,139], C. Lara[61], A. Lardeux[15], A. Lattuca[26], E. Laudi[36], R. Lea[25], L. Leardini[95], S. Lee[140], F. Lehas[84], S. Lehner[114], R.C. Lemmon[85], V. Lenti[105], E. Leogrande[55], I. León Monzón[121], H. León Vargas[65], M. Leoncino[26], P. Lévai[138], S. Li[7,72], X. Li[14], J. Lien[42], R. Lietava[103], S. Lindal[21], V. Lindenstruth[43], C. Lippmann[99], M.A. Lisa[19], H.M. Ljunggren[34], D.F. Lodato[55], P.I. Loenne[22], V. Loginov[77], C. Loizides[76], X. Lopez[72], E. López Torres[9], A. Lowe[138], P. Luettig[62], M. Lunardon[29], G. Luparello[25], M. Lupi[36], T.H. Lutz[139], A. Maevskaya[54], M. Mager[36], S. Mahajan[93], S.M. Mahmood[21], A. Maire[66], R.D. Majka[139], M. Malaev[88], I. Maldonado Cervantes[64], L. Malinina[IV,68], D. Mal'Kevich[56], P. Malzacher[99], A. Mamonov[101], V. Manko[82], F. Manso[72], V. Manzari[36,105], Y. Mao[7], M. Marchisone[26,67,128], J. Mareš[58], G.V. Margagliotti[25], A. Margotti[106], J. Margutti[55], A. Marín[99], C. Markert[120], M. Marquard[62], N.A. Martin[99], P. Martinengo[36], M.I. Martínez[2], G. Martínez García[115], M. Martinez Pedreira[36], A. Mas[122], S. Masciocchi[99], M. Masera[26], A. Masoni[107], A. Mastroserio[33], A. Matyja[119], C. Mayer[119], J. Mazer[127], M. Mazzilli[33], M.A. Mazzoni[110], F. Meddi[23], Y. Melikyan[77], A. Menchaca-Rocha[65], E. Meninno[30], J. Mercado Pérez[95], M. Meres[39], S. Mhlanga[92], Y. Miake[130], M.M. Mieskolainen[47], K. Mikhaylov[56,68], L. Milano[36,76], J. Milosevic[21], A. Mischke[55], A.N. Mishra[50], T. Mishra[59], D. Miśkowiec[99], J. Mitra[135], C.M. Mitu[60], N. Mohammadi[55], B. Mohanty[81], L. Molnar[66], L. Montaño Zetina[11], E. Montes[10], D.A. Moreira De Godoy[63], L.A.P. Moreno[2], S. Moretto[29], A. Morreale[115], A. Morsch[36], V. Muccifora[74], E. Mudnic[118], D. Mühlheim[63], S. Muhuri[135], M. Mukherjee[135], J.D. Mulligan[139], M.G. Munhoz[122], K. Münning[46], R.H. Munzer[37,62,96], H. Murakami[129], S. Murray[67], L. Musa[36], J. Musinsky[57], B. Naik[49], R. Nair[79], B.K. Nandi[49], R. Nania[106], E. Nappi[105], M.U. Naru[16], H. Natal da Luz[122], C. Nattrass[127], S.R. Navarro[2], K. Nayak[81], R. Nayak[49], T.K. Nayak[135], S. Nazarenko[101], A. Nedosekin[56], R.A. Negrao De Oliveira[36], L. Nellen[64], F. Ng[124], M. Nicassio[99], M. Niculescu[60], J. Niedziela[36], B.S. Nielsen[83], S. Nikolaev[82], S. Nikulin[82], V. Nikulin[88], F. Noferini[12,106], P. Nomokonov[68], G. Nooren[55], J.C.C. Noris[2], J. Norman[126], A. Nyanin[82], J. Nystrand[22], H. Oeschler[95], S. Oh[139], S.K. Oh[69], A. Ohlson[36], A. Okatan[71], T. Okubo[48], J. Oleniacz[136], A.C. Oliveira Da Silva[122], M.H. Oliver[139], J. Onderwaater[99], C. Oppedisano[112], R. Orava[47], M. Oravec[117], A. Ortiz Velasquez[64], A. Oskarsson[34], J. Otwinowski[119], K. Oyama[78,95], M. Ozdemir[62], Y. Pachmayer[95], D. Pagano[133], P. Pagano[30], G. Paić[64], S.K. Pal[135], P. Palni[7], J. Pan[137], A.K. Pandey[49], V. Papikyan[1], G.S. Pappalardo[108], P. Pareek[50], W.J. Park[99], S. Parmar[90], A. Passfeld[63],

V. Paticchio[105], R.N. Patra[135], B. Paul[112], H. Pei[7], T. Peitzmann[55], X. Peng[7], H. Pereira Da Costa[15], D. Peresunko[77,82], E. Perez Lezama[62], V. Peskov[62], Y. Pestov[5], V. Petráček[40], V. Petrov[113], M. Petrovici[80], C. Petta[28], S. Piano[111], M. Pikna[39], P. Pillot[115], L.O.D.L. Pimentel[83], O. Pinazza[36,106], L. Pinsky[124], D.B. Piyarathna[124], M. Płoskoń[76], M. Planinic[131], J. Pluta[136], S. Pochybova[138], P.L.M. Podesta-Lerma[121], M.G. Poghosyan[87], B. Polichtchouk[113], N. Poljak[131], W. Poonsawat[116], A. Pop[80], H. Poppenborg[63], S. Porteboeuf-Houssais[72], J. Porter[76], J. Pospisil[86], S.K. Prasad[4], R. Preghenella[36,106], F. Prino[112], C.A. Pruneau[137], I. Pshenichnov[54], M. Puccio[26], G. Puddu[24], P. Pujahari[137], V. Punin[101], J. Putschke[137], H. Qvigstad[21], A. Rachevski[111], S. Raha[4], S. Rajput[93], J. Rak[125], A. Rakotozafindrabe[15], L. Ramello[32], F. Rami[66], R. Raniwala[94], S. Raniwala[94], S.S. Räsänen[47], B.T. Rascanu[62], D. Rathee[90], I. Ravasenga[26], K.F. Read[87,127], K. Redlich[79], R.J. Reed[137], A. Rehman[22], P. Reichelt[62], F. Reidt[36,95], X. Ren[7], R. Renfordt[62], A.R. Reolon[74], A. Reshetin[54], K. Reygers[95], V. Riabov[88], R.A. Ricci[75], T. Richert[34], M. Richter[21], P. Riedler[36], W. Riegler[36], F. Riggi[28], C. Ristea[60], M. Rodríguez Cahuantzi[2], A. Rodriguez Manso[84], K. Røed[21], E. Rogochaya[68], D. Rohr[43], D. Röhrich[22], F. Ronchetti[36,74], L. Ronflette[115], P. Rosnet[72], A. Rossi[29], F. Roukoutakis[91], A. Roy[50], C. Roy[66], P. Roy[102], A.J. Rubio Montero[10], R. Rui[25], R. Russo[26], E. Ryabinkin[82], Y. Ryabov[88], A. Rybicki[119], S. Saarinen[47], S. Sadhu[135], S. Sadovsky[113], K. Šafařík[36], B. Sahlmuller[62], P. Sahoo[50], R. Sahoo[50], S. Sahoo[59], P.K. Sahu[59], J. Saini[135], S. Sakai[74], M.A. Saleh[137], J. Salzwedel[19], S. Sambyal[93], V. Samsonov[77,88], L. Šándor[57], A. Sandoval[65], M. Sano[130], D. Sarkar[135], N. Sarkar[135], P. Sarma[45], E. Scapparone[106], F. Scarlassara[29], C. Schiaua[80], R. Schicker[95], C. Schmidt[99], H.R. Schmidt[35], M. Schmidt[35], S. Schuchmann[62,95], J. Schukraft[36], Y. Schutz[36,115], K. Schwarz[99], K. Schweda[99], G. Scioli[27], E. Scomparin[112], R. Scott[127], M. Šefčík[41], J.E. Seger[89], Y. Sekiguchi[129], D. Sekihata[48], I. Selyuzhenkov[99], K. Senosi[67], S. Senyukov[3,36], E. Serradilla[10,65], A. Sevcenco[60], A. Shabanov[54], A. Shabetai[115], O. Shadura[3], R. Shahoyan[36], A. Shangaraev[113], A. Sharma[93], M. Sharma[93], M. Sharma[93], N. Sharma[127], A.I. Sheikh[135], K. Shigaki[48], Q. Shou[7], K. Shtejer[9,26], Y. Sibiriak[82], S. Siddhanta[107], K.M. Sielewicz[36], T. Siemiarczuk[79], D. Silvermyr[34], C. Silvestre[73], G. Simatovic[131], G. Simonetti[36], R. Singaraju[135], R. Singh[81], V. Singhal[135], T. Sinha[102], B. Sitar[39], M. Sitta[32], T.B. Skaali[21], M. Slupecki[125], N. Smirnov[139], R.J.M. Snellings[55], T.W. Snellman[125], J. Song[98], M. Song[140], Z. Song[7], F. Soramel[29], S. Sorensen[127], F. Sozzi[99], E. Spiriti[74], I. Sputowska[119], M. Spyropoulou-Stassinaki[91], J. Stachel[95], I. Stan[60], P. Stankus[87], E. Stenlund[34], G. Steyn[67], J.H. Stiller[95], D. Stocco[115], P. Strmen[39], A.A.P. Suaide[122], T. Sugitate[48], C. Suire[53], M. Suleymanov[16], M. Suljic[I,25], R. Sultanov[56], M. Šumbera[86], S. Sumowidagdo[51], S. Swain[59], A. Szabo[39], I. Szarka[39], A. Szczepankiewicz[136], M. Szymanski[136], U. Tabassam[16], J. Takahashi[123], G.J. Tambave[22], N. Tanaka[130], M. Tarhini[53], M. Tariq[18], M.G. Tarzila[80], A. Tauro[36], G. Tejeda Muñoz[2], A. Telesca[36], K. Terasaki[129], C. Terrevoli[29], B. Teyssier[132], J. Thäder[76], D. Thakur[50], D. Thomas[120], R. Tieulent[132], A. Tikhonov[54], A.R. Timmins[124], A. Toia[62], S. Trogolo[26], G. Trombetta[33], V. Trubnikov[3], W.H. Trzaska[125], T. Tsuji[129], A. Tumkin[101], R. Turrisi[109], T.S. Tveter[21], K. Ullaland[22], A. Uras[132], G.L. Usai[24], A. Utrobicic[131], M. Vala[57], L. Valencia Palomo[72], J. Van Der Maarel[55], J.W. Van Hoorne[36,114], M. van Leeuwen[55], T. Vanat[86], P. Vande Vyvre[36], D. Varga[138], A. Vargas[2], M. Vargyas[125], R. Varma[49], M. Vasileiou[91], A. Vasiliev[82], A. Vauthier[73], O. Vázquez Doce[37,96], V. Vechernin[134], A.M. Veen[55], A. Velure[22], E. Vercellin[26], S. Vergara Limón[2], R. Vernet[8], L. Vickovic[118], J. Viinikainen[125], Z. Vilakazi[128], O. Villalobos Baillie[103], A. Villatoro Tello[2], A. Vinogradov[82], L. Vinogradov[134], T. Virgili[30], V. Vislavicius[34], Y.P. Viyogi[135], A. Vodopyanov[68], M.A. Völkl[95], K. Voloshin[56], S.A. Voloshin[137], G. Volpe[33,138], B. von Haller[36], I. Vorobyev[37,96], D. Vranic[36,99], J. Vrláková[41], B. Vulpescu[72], B. Wagner[22], J. Wagner[99], H. Wang[55], M. Wang[7], D. Watanabe[130], Y. Watanabe[129], M. Weber[36,114], S.G. Weber[99], D.F. Weiser[95], J.P. Wessels[63], U. Westerhoff[63], A.M. Whitehead[92], J. Wiechula[35], J. Wikne[21], G. Wilk[79], J. Wilkinson[95], G.A. Willems[63], M.C.S. Williams[106], B. Windelband[95], M. Winn[95], S. Yalcin[71], P. Yang[7], S. Yano[48], Z. Yin[7], H. Yokoyama[130], I.-K. Yoo[98], J.H. Yoon[52], V. Yurchenko[3], A. Zaborowska[136], V. Zaccolo[83], A. Zaman[16], C. Zampolli[36,106], H.J.C. Zanoli[122], S. Zaporozhets[68], N. Zardoshti[103], A. Zarochentsev[134], P. Závada[58], N. Zaviyalov[101], H. Zbroszczyk[136], I.S. Zgura[60], M. Zhalov[88], H. Zhang[7,22], X. Zhang[7,76], Y. Zhang[7], C. Zhang[55], Z. Zhang[7], C. Zhao[21], N. Zhigareva[56], D. Zhou[7], Y. Zhou[83], Z. Zhou[22], H. Zhu[7,22], J. Zhu[7,115], A. Zichichi[12,27], A. Zimmermann[95], M.B. Zimmermann[36,63], G. Zinovjev[3], M. Zyzak[43]

Affiliation Notes

[I] Deceased
[II] Also at: Georgia State University, Atlanta, Georgia, United States
[III] Also at Department of Applied Physics, Aligarh Muslim University, Aligarh, India
[IV] Also at: M.V. Lomonosov Moscow State University, D.V. Skobeltsyn Institute of Nuclear, Physics, Moscow, Russia

Collaboration Institutes

[1] A.I. Alikhanyan National Science Laboratory (Yerevan Physics Institute) Foundation, Yerevan, Armenia
[2] Benemérita Universidad Autónoma de Puebla, Puebla, Mexico
[3] Bogolyubov Institute for Theoretical Physics, Kiev, Ukraine
[4] Bose Institute, Department of Physics and Centre for Astroparticle Physics and Space Science (CAPSS), Kolkata, India
[5] Budker Institute for Nuclear Physics, Novosibirsk, Russia
[6] California Polytechnic State University, San Luis Obispo, California, United States
[7] Central China Normal University, Wuhan, China
[8] Centre de Calcul de l'IN2P3, Villeurbanne, France
[9] Centro de Aplicaciones Tecnológicas y Desarrollo Nuclear (CEADEN), Havana, Cuba
[10] Centro de Investigaciones Energéticas Medioambientales y Tecnológicas (CIEMAT), Madrid, Spain
[11] Centro de Investigación y de Estudios Avanzados (CINVESTAV), Mexico City and Mérida, Mexico
[12] Centro Fermi - Museo Storico della Fisica e Centro Studi e Ricerche "Enrico Fermi", Rome, Italy
[13] Chicago State University, Chicago, Illinois, USA
[14] China Institute of Atomic Energy, Beijing, China
[15] Commissariat à l'Energie Atomique, IRFU, Saclay, France
[16] COMSATS Institute of Information Technology (CIIT), Islamabad, Pakistan
[17] Departamento de Física de Partículas and IGFAE, Universidad de Santiago de Compostela, Santiago de Compostela, Spain
[18] Department of Physics, Aligarh Muslim University, Aligarh, India
[19] Department of Physics, Ohio State University, Columbus, Ohio, United States
[20] Department of Physics, Sejong University, Seoul, South Korea
[21] Department of Physics, University of Oslo, Oslo, Norway
[22] Department of Physics and Technology, University of Bergen, Bergen, Norway
[23] Dipartimento di Fisica dell'Università 'La Sapienza' and Sezione INFN Rome, Italy
[24] Dipartimento di Fisica dell'Università and Sezione INFN, Cagliari, Italy
[25] Dipartimento di Fisica dell'Università and Sezione INFN, Trieste, Italy
[26] Dipartimento di Fisica dell'Università and Sezione INFN, Turin, Italy
[27] Dipartimento di Fisica e Astronomia dell'Università and Sezione INFN, Bologna, Italy
[28] Dipartimento di Fisica e Astronomia dell'Università and Sezione INFN, Catania, Italy
[29] Dipartimento di Fisica e Astronomia dell'Università and Sezione INFN, Padova, Italy
[30] Dipartimento di Fisica 'E.R. Caianiello' dell'Università and Gruppo Collegato INFN, Salerno, Italy
[31] Dipartimento DISAT del Politecnico and Sezione INFN, Turin, Italy
[32] Dipartimento di Scienze e Innovazione Tecnologica dell'Università del Piemonte Orientale and Gruppo Collegato INFN, Alessandria, Italy
[33] Dipartimento Interateneo di Fisica 'M. Merlin' and Sezione INFN, Bari, Italy

[34] Division of Experimental High Energy Physics, University of Lund, Lund, Sweden
[35] Eberhard Karls Universität Tübingen, Tübingen, Germany
[36] European Organization for Nuclear Research (CERN), Geneva, Switzerland
[37] Excellence Cluster Universe, Technische Universität München, Munich, Germany
[38] Faculty of Engineering, Bergen University College, Bergen, Norway
[39] Faculty of Mathematics, Physics and Informatics, Comenius University, Bratislava, Slovakia
[40] Faculty of Nuclear Sciences and Physical Engineering, Czech Technical University in Prague, Prague, Czech Republic
[41] Faculty of Science, P.J. Šafárik University, Košice, Slovakia
[42] Faculty of Technology, Buskerud and Vestfold University College, Vestfold, Norway
[43] Frankfurt Institute for Advanced Studies, Johann Wolfgang Goethe-Universität Frankfurt, Frankfurt, Germany
[44] Gangneung-Wonju National University, Gangneung, South Korea
[45] Gauhati University, Department of Physics, Guwahati, India
[46] Helmholtz-Institut für Strahlen- und Kernphysik, Rheinische Friedrich-Wilhelms-Universität Bonn, Bonn, Germany
[47] Helsinki Institute of Physics (HIP), Helsinki, Finland
[48] Hiroshima University, Hiroshima, Japan
[49] Indian Institute of Technology Bombay (IIT), Mumbai, India
[50] Indian Institute of Technology Indore, Indore (IITI), India
[51] Indonesian Institute of Sciences, Jakarta, Indonesia
[52] Inha University, Incheon, South Korea
[53] Institut de Physique Nucléaire d'Orsay (IPNO), Université Paris-Sud, CNRS-IN2P3, Orsay, France
[54] Institute for Nuclear Research, Academy of Sciences, Moscow, Russia
[55] Institute for Subatomic Physics of Utrecht University, Utrecht, Netherlands
[56] Institute for Theoretical and Experimental Physics, Moscow, Russia
[57] Institute of Experimental Physics, Slovak Academy of Sciences, Košice, Slovakia
[58] Institute of Physics, Academy of Sciences of the Czech Republic, Prague, Czech Republic
[59] Institute of Physics, Bhubaneswar, India
[60] Institute of Space Science (ISS), Bucharest, Romania
[61] Institut für Informatik, Johann Wolfgang Goethe-Universität Frankfurt, Frankfurt, Germany
[62] Institut für Kernphysik, Johann Wolfgang Goethe-Universität Frankfurt, Frankfurt, Germany
[63] Institut für Kernphysik, Westfälische Wilhelms-Universität Münster, Münster, Germany
[64] Instituto de Ciencias Nucleares, Universidad Nacional Autónoma de México, Mexico City, Mexico
[65] Instituto de Física, Universidad Nacional Autónoma de México, Mexico City, Mexico
[66] Institut Pluridisciplinaire Hubert Curien (IPHC), Université de Strasbourg, CNRS-IN2P3, Strasbourg, France
[67] iThemba LABS, National Research Foundation, Somerset West, South Africa
[68] Joint Institute for Nuclear Research (JINR), Dubna, Russia
[69] Konkuk University, Seoul, South Korea
[70] Korea Institute of Science and Technology Information, Daejeon, South Korea
[71] KTO Karatay University, Konya, Turkey
[72] Laboratoire de Physique Corpusculaire (LPC), Clermont Université, Université Blaise Pascal, CNRS–IN2P3, Clermont-Ferrand, France
[73] Laboratoire de Physique Subatomique et de Cosmologie, Université Grenoble-Alpes, CNRS-IN2P3, Grenoble, France
[74] Laboratori Nazionali di Frascati, INFN, Frascati, Italy
[75] Laboratori Nazionali di Legnaro, INFN, Legnaro, Italy
[76] Lawrence Berkeley National Laboratory, Berkeley, California, United States
[77] Moscow Engineering Physics Institute, Moscow, Russia

[78] Nagasaki Institute of Applied Science, Nagasaki, Japan
[79] National Centre for Nuclear Studies, Warsaw, Poland
[80] National Institute for Physics and Nuclear Engineering, Bucharest, Romania
[81] National Institute of Science Education and Research, Bhubaneswar, India
[82] National Research Centre Kurchatov Institute, Moscow, Russia
[83] Niels Bohr Institute, University of Copenhagen, Copenhagen, Denmark
[84] Nikhef, Nationaal instituut voor subatomaire fysica, Amsterdam, Netherlands
[85] Nuclear Physics Group, STFC Daresbury Laboratory, Daresbury, United Kingdom
[86] Nuclear Physics Institute, Academy of Sciences of the Czech Republic, Řež u Prahy, Czech Republic
[87] Oak Ridge National Laboratory, Oak Ridge, Tennessee, United States
[88] Petersburg Nuclear Physics Institute, Gatchina, Russia
[89] Physics Department, Creighton University, Omaha, Nebraska, United States
[90] Physics Department, Panjab University, Chandigarh, India
[91] Physics Department, University of Athens, Athens, Greece
[92] Physics Department, University of Cape Town, Cape Town, South Africa
[93] Physics Department, University of Jammu, Jammu, India
[94] Physics Department, University of Rajasthan, Jaipur, India
[95] Physikalisches Institut, Ruprecht-Karls-Universität Heidelberg, Heidelberg, Germany
[96] Physik Department, Technische Universität München, Munich, Germany
[97] Purdue University, West Lafayette, Indiana, United States
[98] Pusan National University, Pusan, South Korea
[99] Research Division and ExtreMe Matter Institute EMMI, GSI Helmholtzzentrum für Schwerionenforschung, Darmstadt, Germany
[100] Rudjer Bošković Institute, Zagreb, Croatia
[101] Russian Federal Nuclear Center (VNIIEF), Sarov, Russia
[102] Saha Institute of Nuclear Physics, Kolkata, India
[103] School of Physics and Astronomy, University of Birmingham, Birmingham, United Kingdom
[104] Sección Física, Departamento de Ciencias, Pontificia Universidad Católica del Perú, Lima, Peru
[105] Sezione INFN, Bari, Italy
[106] Sezione INFN, Bologna, Italy
[107] Sezione INFN, Cagliari, Italy
[108] Sezione INFN, Catania, Italy
[109] Sezione INFN, Padova, Italy
[110] Sezione INFN, Rome, Italy
[111] Sezione INFN, Trieste, Italy
[112] Sezione INFN, Turin, Italy
[113] SSC IHEP of NRC Kurchatov institute, Protvino, Russia
[114] Stefan Meyer Institut für Subatomare Physik (SMI), Vienna, Austria
[115] SUBATECH, Ecole des Mines de Nantes, Université de Nantes, CNRS-IN2P3, Nantes, France
[116] Suranaree University of Technology, Nakhon Ratchasima, Thailand
[117] Technical University of Košice, Košice, Slovakia
[118] Technical University of Split FESB, Split, Croatia
[119] The Henryk Niewodniczanski Institute of Nuclear Physics, Polish Academy of Sciences, Cracow, Poland
[120] The University of Texas at Austin, Physics Department, Austin, Texas, USA
[121] Universidad Autónoma de Sinaloa, Culiacán, Mexico
[122] Universidade de São Paulo (USP), São Paulo, Brazil
[123] Universidade Estadual de Campinas (UNICAMP), Campinas, Brazil
[124] University of Houston, Houston, Texas, United States
[125] University of Jyväskylä, Jyväskylä, Finland

[126] University of Liverpool, Liverpool, United Kingdom
[127] University of Tennessee, Knoxville, Tennessee, United States
[128] University of the Witwatersrand, Johannesburg, South Africa
[129] University of Tokyo, Tokyo, Japan
[130] University of Tsukuba, Tsukuba, Japan
[131] University of Zagreb, Zagreb, Croatia
[132] Université de Lyon, Université Lyon 1, CNRS/IN2P3, IPN-Lyon, Villeurbanne, France
[133] Università di Brescia
[134] V. Fock Institute for Physics, St. Petersburg State University, St. Petersburg, Russia
[135] Variable Energy Cyclotron Centre, Kolkata, India
[136] Warsaw University of Technology, Warsaw, Poland
[137] Wayne State University, Detroit, Michigan, United States
[138] Wigner Research Centre for Physics, Hungarian Academy of Sciences, Budapest, Hungary
[139] Yale University, New Haven, Connecticut, United States
[140] Yonsei University, Seoul, South Korea
[141] Zentrum für Technologietransfer und Telekommunikation (ZTT), Fachhochschule Worms, Worms, Germany